

Article

GWBASE – An Algorithm for Assessing the Impact of Groundwater Decline on Baseflow in US Streams

Xueyi Li¹, Norman L. Jones^{1,*} and Gustavious P. Williams¹, Amin Aghababaei¹, Riley C. Hales¹

¹ Civil and Construction Engineering, Brigham Young University; xueyil@student.byu.edu (X.L.); njones@byu.edu (N.L.J.); gus.p.williams@byu.edu (G.P.W.); aghababa@student.byu.edu (A.A.); rchales@byu.edu (R.C.H.)

* Correspondence: njones@byu.edu; Tel.: (+1-801-422-7569)

Abstract

A single paragraph of about 200 words maximum. For research articles, abstracts should give a pertinent overview of the work. We strongly encourage authors to use the following style of structured abstracts, but without headings: (1) Background: Place the question addressed in a broad context and highlight the purpose of the study; (2) Methods: briefly describe the main methods or treatments applied; (3) Results: summarize the article's main findings; (4) Conclusions: indicate the main conclusions or interpretations. The abstract should be an objective representation of the article and it must not contain results that are not presented and substantiated in the main text and should not exaggerate the main conclusions.

Keywords: groundwater, baseflow, drought

Academic Editor: Firstname Lastname

Received: date

Revised: date

Accepted: date

Published: date

Citation: To be added by editorial staff during production.

Copyright: © 2025 by the authors. Submitted for possible open access publication under the terms and conditions of the Creative Commons Attribution (CC BY) license (<https://creativecommons.org/licenses/by/4.0/>).

1. Introduction

Baseflow represents the portion of streamflow that is sustained primarily by groundwater discharge during periods of little or no precipitation. It plays a critical role in maintaining streamflow continuity, supporting aquatic ecosystems, and regulating water quality. Because baseflow reflects the long-term balance between groundwater recharge and discharge, understanding its variability is fundamental to evaluating watershed resilience under changing climatic and anthropogenic conditions.

Groundwater can be a major contributor to baseflow in many basins, especially in regions with shallow water tables and permeable hydrogeologic formations. Numerous studies have demonstrated that reductions in groundwater storage can directly diminish baseflow, leading to streamflow depletion, reduced ecosystem health, and altered hydrologic regimes [1][2][3]. Recent research has documented widespread declines in groundwater levels across parts of the United States, particularly in intensively irrigated agricultural regions [4][5][6]. Investigations such as the *New York Times* national groundwater assessment and recent studies in the Central Valley of California have highlighted significant long-term declines in water tables and associated streamflow reductions [7]. Other regional analyses have also reported similar trends in declining groundwater storage and reduced baseflow contributions, underscoring the urgency of understanding groundwater–surface water connectivity at large spatial scales. [8]

The United States provides an unparalleled opportunity to study these interactions due to the availability of extensive, high-quality hydrologic observations. The USGS

maintains national networks of both stream gages and groundwater wells, offering decades of concurrent daily streamflow and groundwater level data. This data richness makes it possible to explore groundwater–baseflow relationships systematically across diverse hydroclimatic and geologic settings.

The objective of this study is to develop a generalized algorithm that leverages these national datasets to quantify the relationship between groundwater level variations and baseflow dynamics. Specifically, the algorithm is designed to (1) identify basins where groundwater and baseflow are hydrologically connected, and (2) evaluate how declining groundwater levels influence streamflow during baseflow-dominated periods. We have implemented this algorithm in a Python package called GWBASE.

1.1. Study Area

Although this paper focuses primarily on the methodological development of the GWBASE algorithm, we demonstrate the application of the algorithm within the Great Salt Lake Basin (GSLB) in Utah (Figure 1). The GSLB is a closed hydrologic system in which all surface water drains toward the Great Salt Lake, a terminal lake with no outlet to the ocean. Streamflow is supplied mainly by snowmelt-fed rivers rising in the Wasatch and Uinta mountains, while evaporation accounts for most losses. Annual precipitation ranges from roughly 10–65 cm in the low-elevation valleys to more than 100 cm in the surrounding mountain headwaters, producing strong hydroclimatic gradients and sustained groundwater–surface water exchange [9].

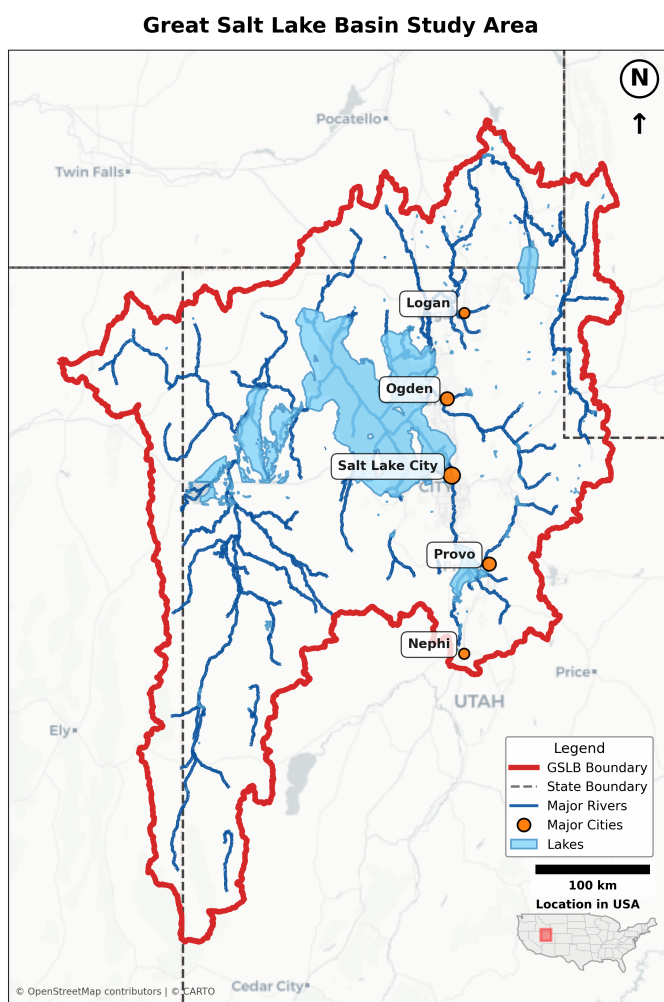


Figure 1. Great Salt Lake Basin (GSLB) study area

The basin has an effective hydrologic area of about 55,000 km² and supports nearly two million residents concentrated in the Salt Lake City–Ogden urban corridor [10]. The lake and its tributaries play key ecological and economic roles, and recent declines in lake level have heightened concern about long-term reductions in inflows. This setting offers a relevant case study for evaluating how groundwater level changes may influence baseflow, and how a national-scale framework could support assessments of groundwater contributions to streamflow under changing hydrologic conditions.

2. Data

This study integrates two national-scale datasets: (1) daily streamflow records from the United States Geological Survey (USGS) stream gaging network, and (2) groundwater level observations from the USGS National Groundwater Monitoring Network (NGWMN). Stream gages were used to delineate streamflow regimes and identify periods of baseflow dominance, while groundwater wells were analyzed to evaluate temporal variations in water table elevation (WTE).

2.1. Groundwater Level Data

Groundwater level data were obtained from the United States Geological Survey (USGS) National Water Information System (NWIS) [11]. NWIS provides long-term observations of groundwater levels from over 850,000 monitoring wells across the United States and contains millions of water level records. Each record includes well location, elevation, and depth to water table. These data were downloaded and processed to obtain water table elevations (WTE) referenced to mean sea level.

Within the Great Salt Lake Basin (GSLB), a total of 8752 wells were identified with usable water-level records. The dataset includes both continuous and intermittent measurements collected from 1906 - 2023. Figure 2 shows the spatial distribution of these wells across the basin. The density of wells varies by subbasin, with higher concentrations in valley regions and fewer records in upland areas. Together, these wells provide a spatially extensive representation of groundwater conditions across the study domain.

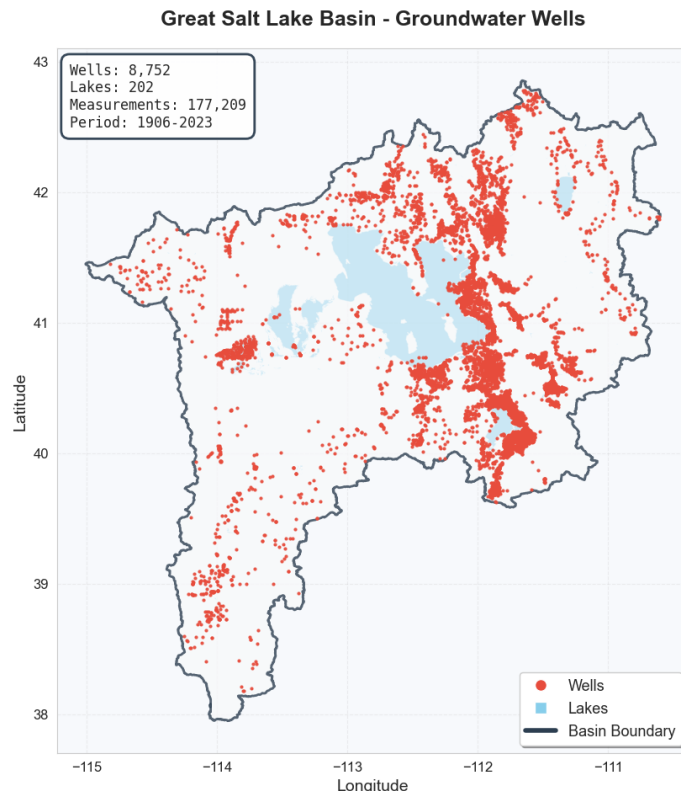


Figure 2. Wells in GSLB

2.2. Streamflow data and gage information

Daily streamflow data were obtained from the U.S. Geological Survey National Water Information System [12]. Observed discharge records were used as the surface water data source for this study. Stream gages with insufficient data coverage were excluded from the analysis.

Stream gage location and network information were obtained from the National Water Model [12]. Gage locations were linked to stream reaches in the National Water Model to identify upstream–downstream relationships and delineate contributing basins. This information was used to support gage selection and to pair stream gages with nearby groundwater wells.

2.3. Hydrography Data

Stream network and catchment boundaries used in this study were obtained from GEOGloWS, which provides globally consistent hydrologic features [13]. The GEOGloWS stream network represents the global river system as a connected set of stream reaches, each with a unique identifier, geometric attributes, and predefined upstream–downstream relationships. Corresponding catchment polygons delineate the contributing drainage area for each stream reach.

Figure 3 presents the spatial layout of major streams and catchments used in this study. Together with the groundwater well data, these datasets form the foundation for the well–gage pairing and analysis described in Section 3.

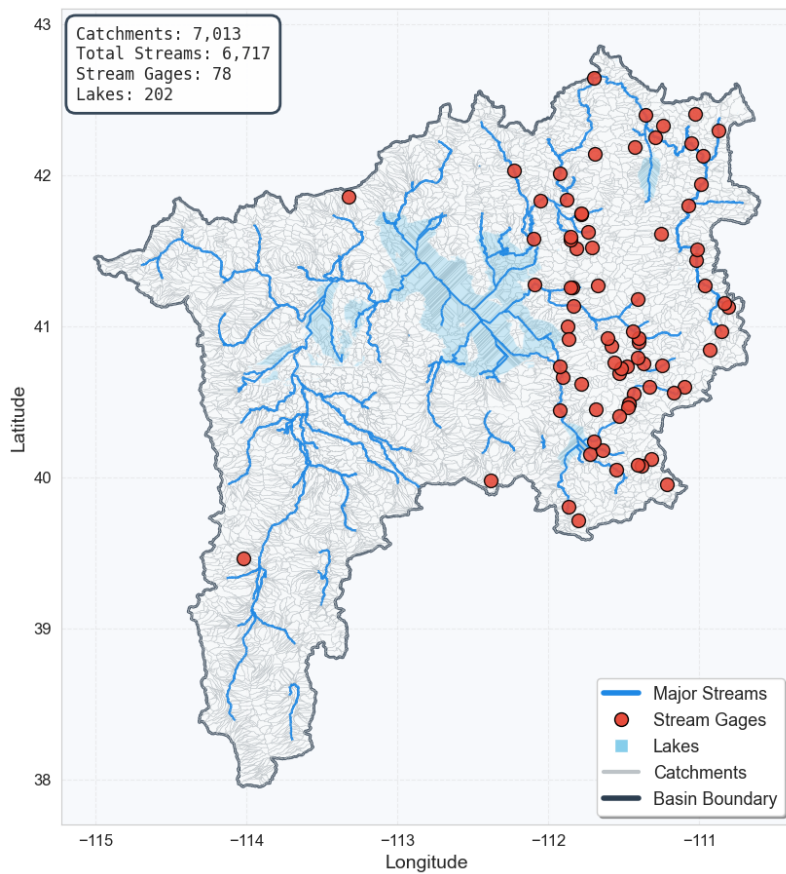


Figure 3. Streams in GSLB

2.4. Baseflow classification label data

Daily streamflow records at each gage were accompanied by a binary indicator identifying baseflow-dominated conditions. This indicator ($BFD = 1$ for baseflow-dominated days and $BFD = 0$ otherwise) was obtained from an externally developed machine-learning classification framework [14]. In this study, the BFD flag was used directly as an input dataset to filter streamflow and groundwater observations, isolating periods when streamflow variability is expected to be primarily controlled by groundwater discharge rather than surface runoff processes.

3. Methods

3.1. Overview

We developed a systematic algorithm to evaluate the relationship between groundwater level variations and streamflow during baseflow-dominated (BFD) periods, which we implemented in a Python package called GWBASE. The GWBASE workflow (Figure 4) integrates spatial pairing between wells and gages, temporal interpolation of groundwater levels, formation of water level change vs. baseflow change data pairs ($\Delta WTE - \Delta Q$), and a statistical analysis of $\Delta WTE - \Delta Q$ relationships. The overall GWBASE workflow is illustrated in INSERT REF. Each of these steps is described in detail in the following section.

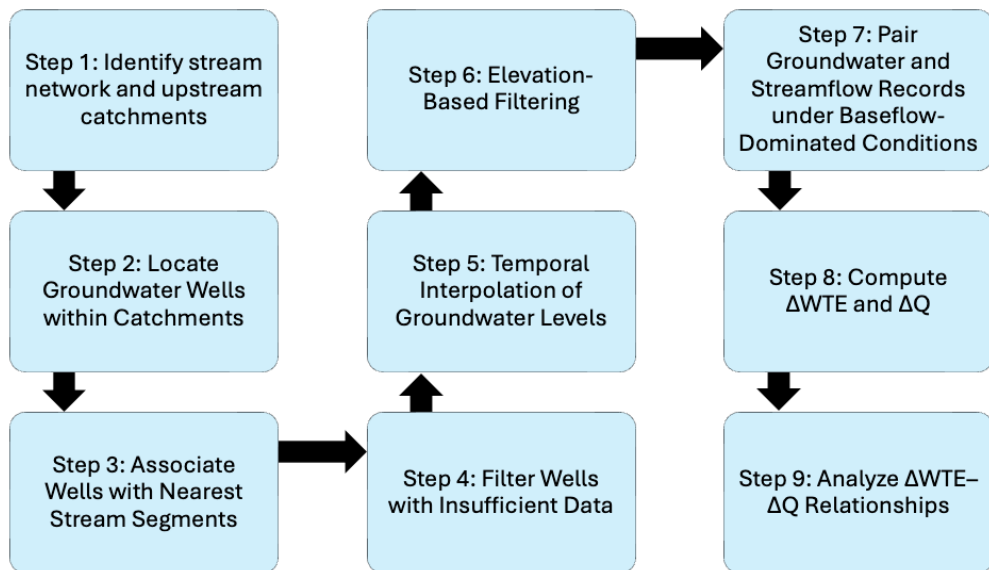


Figure 4. GWBASE workflow

133
134
135
136
137
138
139
140
141
142
143
144
145
146
147
148
149
150
151
152
153
154
155
156
157
158
159
160
161
162
163
164
165

3.2. Algorithm Steps

3.2.1. Step 1: Identify Stream Network and Upstream Catchments

In the first step, stream gages are first matched to catchments by placing each gage's coordinates inside the subbasin polygons. This provides the basic gage–catchment links. In many drainage systems, several gages can exist along the same flow path. If each gage are analyzed separately, their upstream areas would be processed repeatedly. To avoid this, the workflow identifies one terminal gage for each drainage network. A terminal gage is defined here as a gage that has no other gage located downstream.

To identify these terminal locations, the stream network is converted into a directed graph using the catchment connectivity fields in the hydrographic dataset. The upstream catchment ID (LINKNO) and downstream link (DSLINKNO) form the graph structure. Using this representation, downstream paths are checked for every gage-associated catchment. Gages with no downstream path to another gage are classified as terminal. The initial list of terminals is then reviewed and adjusted using hydrologic knowledge to correct for classification errors.

After the terminal gages are determined, their upstream contributing areas are delineated. This is done by tracing all catchments that drain to each terminal gage through the directed network. The result is a set of complete and non-overlapping upstream catchment groups. Groundwater wells are then intersected with these catchments to assign each well to the terminal gage that receives its drainage. These gage–well associations serve as the basis for the later groundwater–streamflow comparison.

Figure 5 illustrates a simple example of how upstream catchments are identified for a terminal gage. In this network, gage A is the most downstream location. Along the main flow path, gage E drains catchment 5 and flows into gage D, which drains catchment 4. Both E and D then flow into gage C, which drains catchment 3. Because C is downstream of both D and E, its upstream area includes catchments 3, 4, and 5. Gage B, located in catchment 2, also flows directly to gage A. Consequently, the total upstream drainage area of gage A consists of catchments 2, 3, 4, and 5 together with its own local catchment (catchment 1). This example shows how the upstream catchment set at any gage is formed by combining its own catchment with those of all upstream gages identified through the flow network.

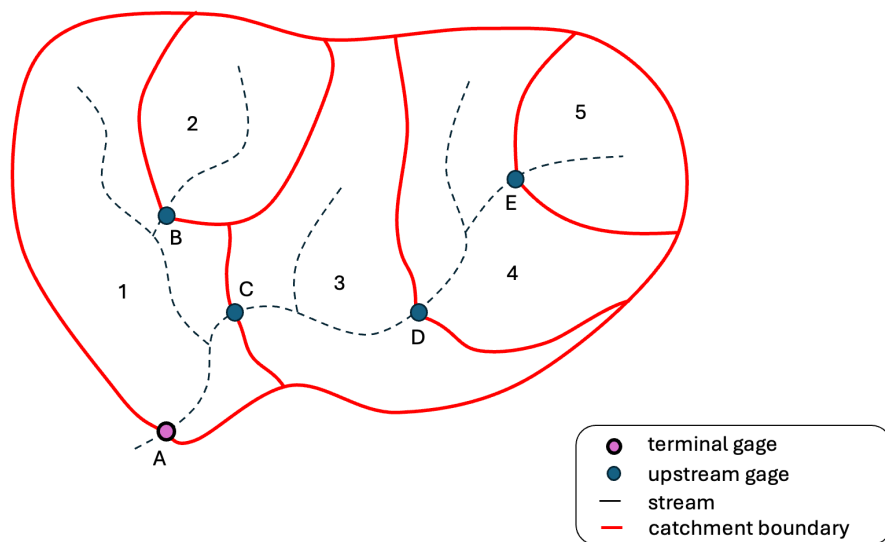


Figure 5. Example drainage network showing terminal and upstream gages, local catchments, and streamflow direction used to delineate contributing areas.

3.2.2. Step 2: Locate Groundwater Wells within Catchments

After the terminal drainage areas are defined, groundwater monitoring wells are spatially matched to the catchments in which they are located. This is done by intersecting well coordinates with catchment boundaries and confirming that each well falls within the expected area. The well locations are then linked to the corresponding terminal gage of the catchment. This produces a consistent set of well-gage pairs that reflects the natural watershed structure and provides the basis for comparing groundwater levels with downstream streamflow.

Figure 6 illustrates the process of locating groundwater wells within a catchment. All wells situated inside the catchment boundary are identified through a point-in-polygon operation. This establishes the set of wells that contribute to the downstream gage and defines the spatial domain for subsequent groundwater–surface water comparison.

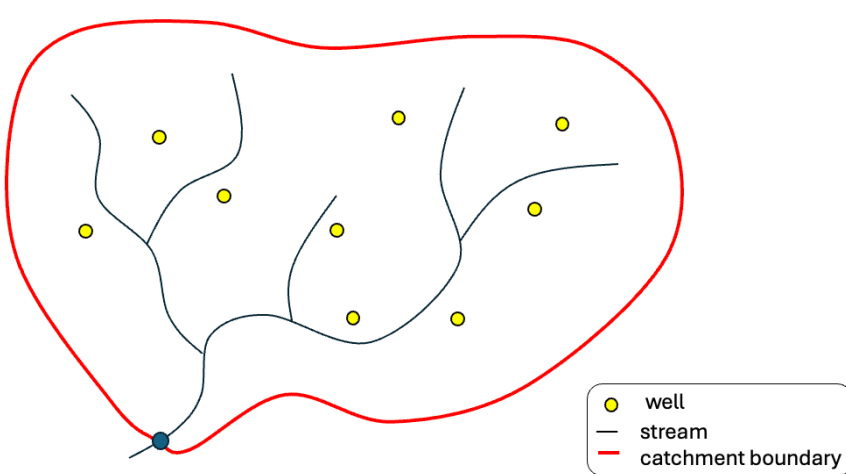


Figure 6. Find catchment area and wells

3.2.3. Step 3: Associate Wells with Nearest Stream Segments

Each well is further associated with the nearest stream segment to establish a more detailed hydrologic connection. Using the hydrographic network, the closest river reach to each well is identified and the corresponding reach identifier and streambed elevation are recorded. These attributes allow elevation-based screening in later steps, where wells with unrealistic vertical separation from the stream are removed. The resulting well-reach linkage ensures that groundwater levels are compared with the most physically relevant part of the stream network.

Figure 7 demonstrates how each well is associated with the nearest stream segment. For every well, the closest reach in the stream network is identified, and the direction of the nearest-distance link is shown. This association ensures that each well is connected to a physically relevant part of the channel network, which is necessary for later elevation-based screening.

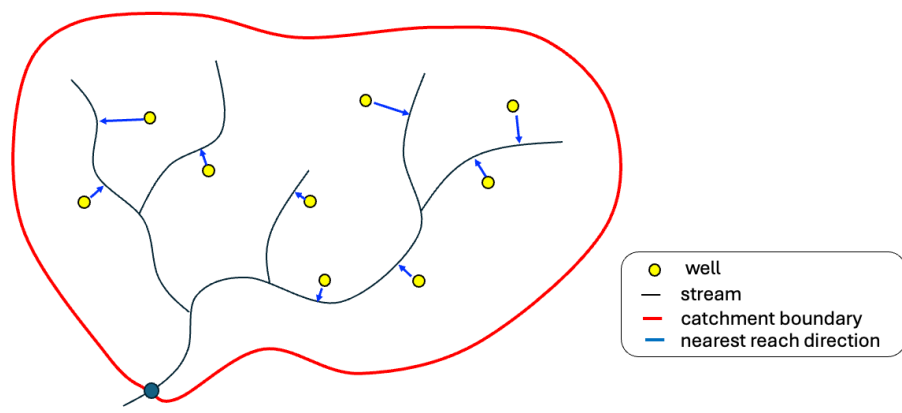


Figure 7. Relate wells to stream segments

3.2.4. Step 4: Filter Wells with Insufficient Data

Groundwater level records are screened to remove well measurements that lack sufficient temporal coverage. A two-stage outlier check is applied, first using a Z-score method with a threshold of 3.0 to identify values that deviate strongly from the mean, and then using an interquartile range filter with a multiplier of 1.5 to remove observations outside the expected data spread. These procedures remove extreme measurements that could affect later interpolation. Wells with fewer than two valid measurements are excluded because they do not provide enough information to represent seasonal or interannual variability. Only wells with adequate data density are retained for further analysis.

3.2.5. Step 5: Temporal Interpolation of Groundwater Levels

Groundwater level time series are interpolated to daily resolution using the Piecewise Cubic Hermite Interpolating Polynomial (PCHIP) method. This approach preserves monotonic patterns between observations and avoids unrealistic oscillations that can occur with traditional spline interpolation. As Figure 8 shown below, for each well, observation dates are converted to numerical time, the PCHIP function is applied between consecutive measurements, and daily values are generated across the entire period of record. Local extrema are preserved, and the resulting time series maintains hydrologic realism. The interpolated results are then combined with well metadata, including location and surface elevation, to form a consistent dataset for later comparison with daily streamflow records.

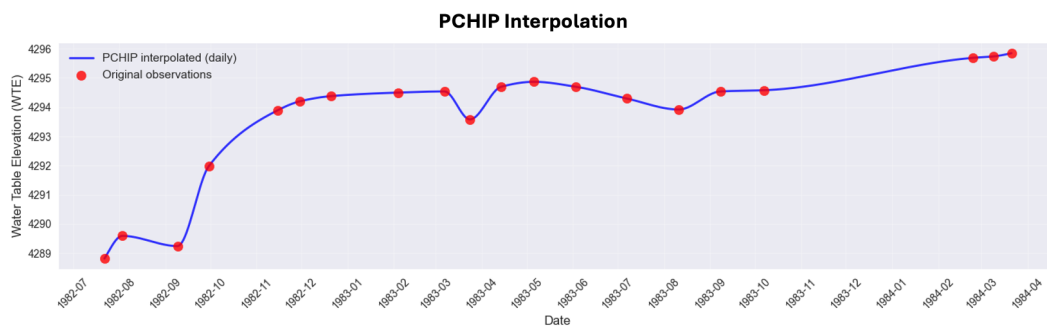


Figure 8. Example of daily groundwater level interpolation using the PCHIP method.

Red points represent original groundwater level observations, and the blue line shows the PCHIP-interpolated daily time series. The method preserves monotonic trends and local extrema while avoiding artificial oscillations.

3.2.6. Step 6: Elevation-Based Filtering

To focus on wells with realistic potential for groundwater and surface water interaction, an elevation-based screening is applied. The logic is that well with water levels far below the stream elevation are not likely to impact baseflow to the stream. For each well, the interpolated water table elevation is compared with the elevation of the nearest stream segment identified in previous steps. Wells with water levels far below the local streambed are removed, since these conditions typically represent deep or confined aquifers with limited influence on streamflow. This procedure retained wells where groundwater levels are close to or higher than the nearby stream channel, reflecting conditions that can support hydrologic exchange.

Figure 9 shows a simple example of the elevation-based filter using a 30 m buffer. The blue line marks the streambed elevation. Wells plotted in the blue or green zones fall within 30 m of the streambed and are kept for analysis. Wells in the red zone lie more than 30 m below the streambed and are removed. This example illustrates how vertical separation is used to decide whether a well is likely to interact with the nearby stream.

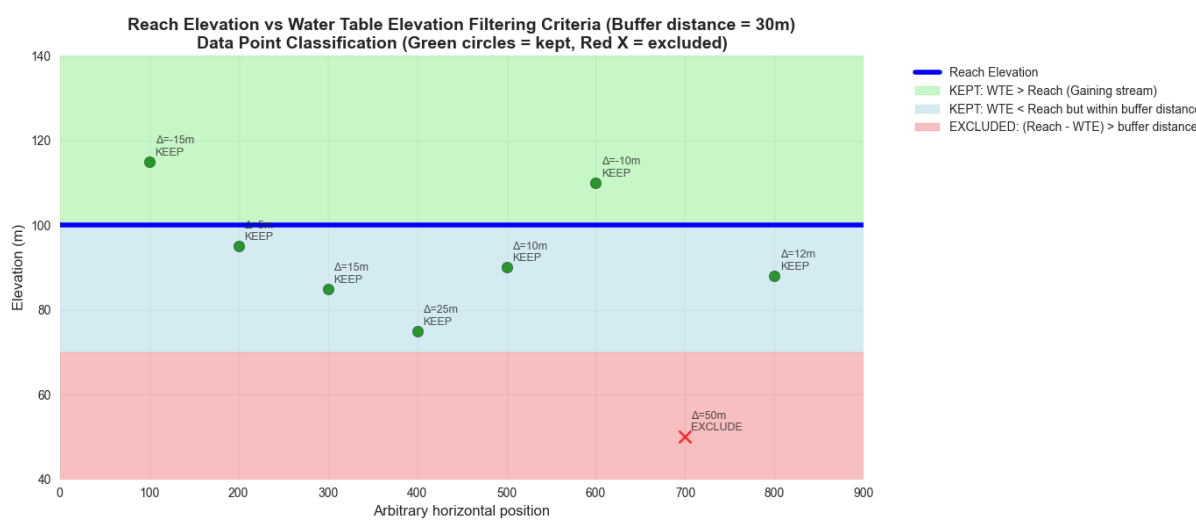


Figure 9. Conceptual illustration of elevation-based well filtering using a 30 m buffer.

The blue line represents the streambed elevation. Wells within 30 m of the streambed (blue and green zones) are retained, while wells more than 30 m below the streambed (red zone) are excluded.

3.2.7. Step 7: Pair Groundwater and Streamflow Records under Baseflow-Dominated Conditions

In our earlier study, we developed a machine learning classifier to identify baseflow-dominated days in daily streamflow records [14]. The classifier labels each day as either baseflow-dominated or non-baseflow by evaluating streamflow behavior, and identifying periods when flow is sustained mainly by groundwater discharge rather than surface runoff.

For all dates labeled as baseflow-dominated, each well's daily water table elevation is paired with the streamflow observed on the same day at the corresponding terminal gage. These paired records represent hydrologic conditions when streamflow is primarily controlled by groundwater discharge, making them suitable for assessing groundwater-surface water connectivity.

3.2.8. Step 8: Compute ΔWTE and ΔQ

For each well-gage pair, the earliest BFD day was selected as the baseline condition, with initial water level (WTE_0) and discharge (Q_0). Subsequent BFD observations were converted to changes relative to the baseline as shown in Equation 1 and Equation 2 :

$$\Delta WTE = WTE - WTE_0 \quad (1)$$

$$\Delta Q = Q - Q_0 \quad (2)$$

To illustrate this procedure, Figure 10 shows an example of a well-gage pair in which the first day classified as baseflow-dominated (BFD=1) is identified as the reference condition. On this date, the well's groundwater elevation (WTE_0) and the gage's stream discharge (Q_0) are marked with gold star symbols in the upper (WTE) and lower (Q) panels, respectively. Horizontal dashed lines indicate the baseline values, and a vertical connector links the two stars, emphasizing that both baseline quantities correspond to the same hydrologic moment. Periods classified as BFD=1 are shaded to highlight the subset of observations used in the subsequent computations. In this zone, each ΔWTE and the corresponding ΔQ are linked to form a dataset of ΔWTE - ΔQ pairs. These pairs form the basis of assessing the impact of rising or falling groundwater levels on baseflow.

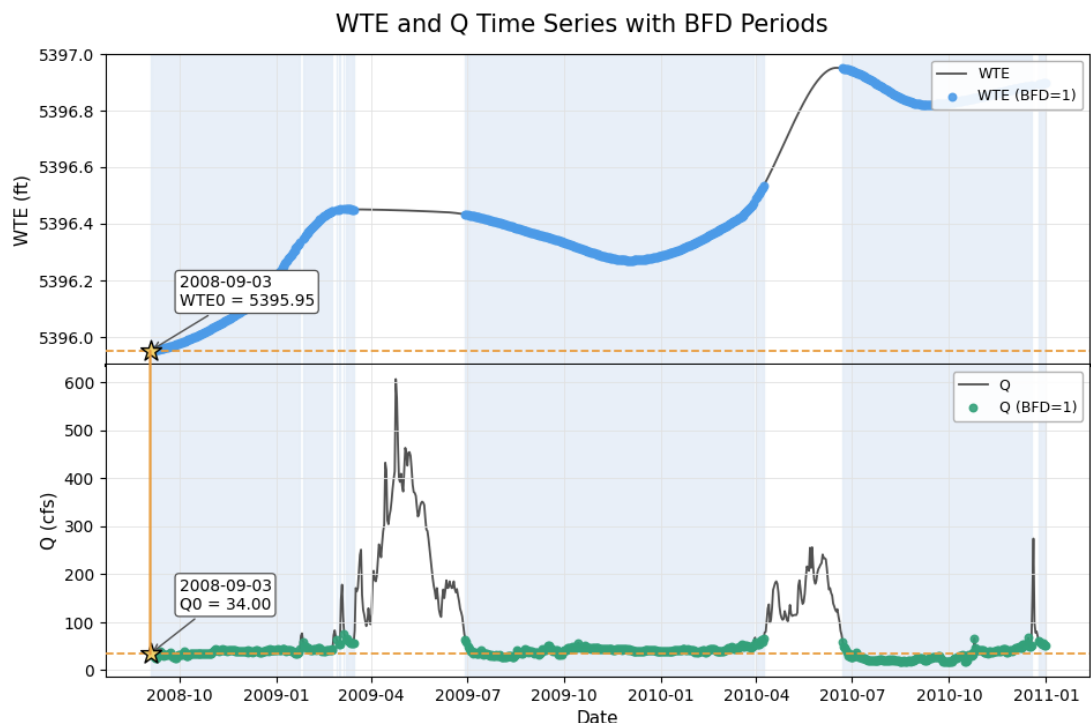


Figure 10. Example time series of groundwater level (WTE) and streamflow (Q) with baseflow-dominated (BFD) periods highlighted.

3.2.9. Step 9: Analyze Δ WTE– Δ Q Relationships

We use simple linear regression to evaluate the relationship between Δ WTE and Δ Q for each well–gage pair during baseflow-dominated periods and to quantify groundwater influence on streamflow. Correlation measures are used to identify wells that exhibit strong hydrologic connectivity. Spatial maps are created to visualize areas with high or low correlation across the study region. In addition, Δ WTE and Δ Q are aggregated by terminal gage and for the complete drainage network to assess collective groundwater-driven changes in streamflow.

3.3. Mutual Information Analysis

Mutual information (MI) is used to quantify the statistical dependence between groundwater level changes (Δ WTE) and streamflow changes (Δ Q) during baseflow-dominated periods. Unlike linear correlation, MI can capture both linear and nonlinear relationships and does not assume a specific functional form between variables.

For two random variables X and Y , mutual information is defined as:

$$I(X; Y) = \sum_{x \in X} \sum_{y \in Y} p(x, y) \log \left(\frac{p(x, y)}{p(x)p(y)} \right) \quad (3)$$

where $p(x, y)$ is the joint probability distribution of X and Y , and $p(x)$ and $p(y)$ are their marginal distributions. Mutual information measures the reduction in uncertainty of one variable given knowledge of the other. A value of zero indicates statistical independence, while larger values indicate stronger dependence.

In this study, MI is computed between Δ WTE and Δ Q for each well–gage pair using data from baseflow-dominated days only. MI is used as a complementary metric to linear regression and correlation, providing additional insight into groundwater–streamflow connectivity when relationships may be nonlinear or heterogeneous across space.

3.4. Cross-correlation function (CCF) analysis

271

272

273

274

275

276

277

278

279

280

281

282

283

284

285

286

287

288

289

290

291

292

293

294

295

296

297

The cross-correlation function (CCF) is used to examine the temporal relationship between groundwater level changes (ΔWTE) and streamflow changes (ΔQ) during baseflow-dominated periods. CCF quantifies the similarity between two time series as a function of time lag and is used to identify delayed groundwater responses in streamflow.

For two time series X_t and Y_t , the cross-correlation at lag k is defined as:

$$\rho_{XY}(k) = \frac{\text{cov}(X_t, Y_{t+k})}{\sigma_X \sigma_Y} \quad (4)$$

where $\text{cov}(\cdot)$ is the covariance between the two series, σ_X and σ_Y are their standard deviations, and k represents the time lag. Positive lag values indicate that changes in groundwater levels precede changes in streamflow, while negative lags indicate the opposite.

In this study, CCF is computed between ΔWTE and ΔQ for each well–gage pair using baseflow-dominated days only. The magnitude of the cross-correlation and the lag at which it peaks are used to assess the strength and timing of groundwater–streamflow interactions.

3.5. Machine learning model

Baseflow-dominated (BFD) periods were identified using a machine-learning classification framework previously developed [14]. The model operates on daily streamflow time series and assigns a binary label to each day, where $BFD = 1$ indicates conditions dominated by groundwater discharge and $BFD = 0$ denotes periods influenced by surface runoff or event flow.

The classifier was trained using hydrologically relevant features derived from streamflow dynamics, enabling it to distinguish recession-driven baseflow behavior from event-driven responses across a wide range of hydrologic regimes. Model performance and generalizability were evaluated in the original study using multiple gages and independent validation datasets.

In the present work, the resulting BFD classifications were applied to each gage to filter streamflow and groundwater observations. Subsequent analyses were restricted to $BFD = 1$ periods, ensuring that inferred relationships between groundwater levels and streamflow reflect baseflow-controlled conditions rather than transient runoff responses. Figure 11 illustrates an example hydrograph with BFD periods highlighted.

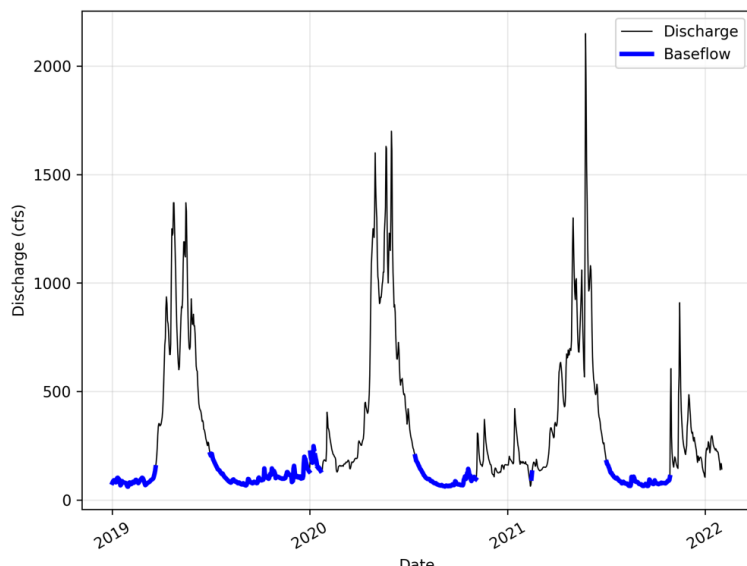


Figure 11. Baseflow Dominant Flows (0-1)

4. Results

We use the Great Salt Lake Basin (GSLB) as a case study to demonstrate our analytical framework. After applying the terminal gage identification algorithm, we identified 12 terminal gages in GSLB (Figure 12). These terminal gages represent the most downstream monitoring locations in their respective sub-watersheds, capturing the integrated hydrologic response of their contributing areas.

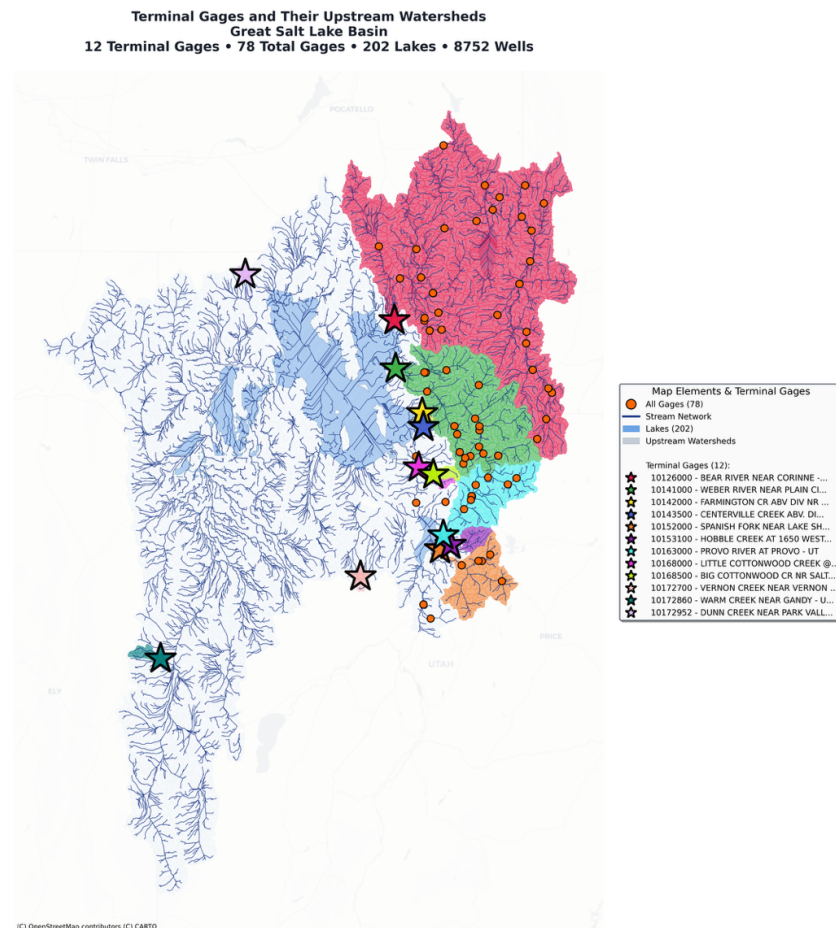


Figure 12. Overview map

After data filtering based on data availability and quality criteria, only 6 of the 12 terminal gages retained sufficient concurrent streamflow and water table elevation (WTE) data to conduct the paired analysis. A representative subbasin is shown in Figure 13. The yellow star represents the terminal gage location where the Bear River gage is situated. The orange dots indicate additional streamflow gaging stations in the upstream network, and the brown squares represent groundwater monitoring wells distributed throughout the contributing watershed.

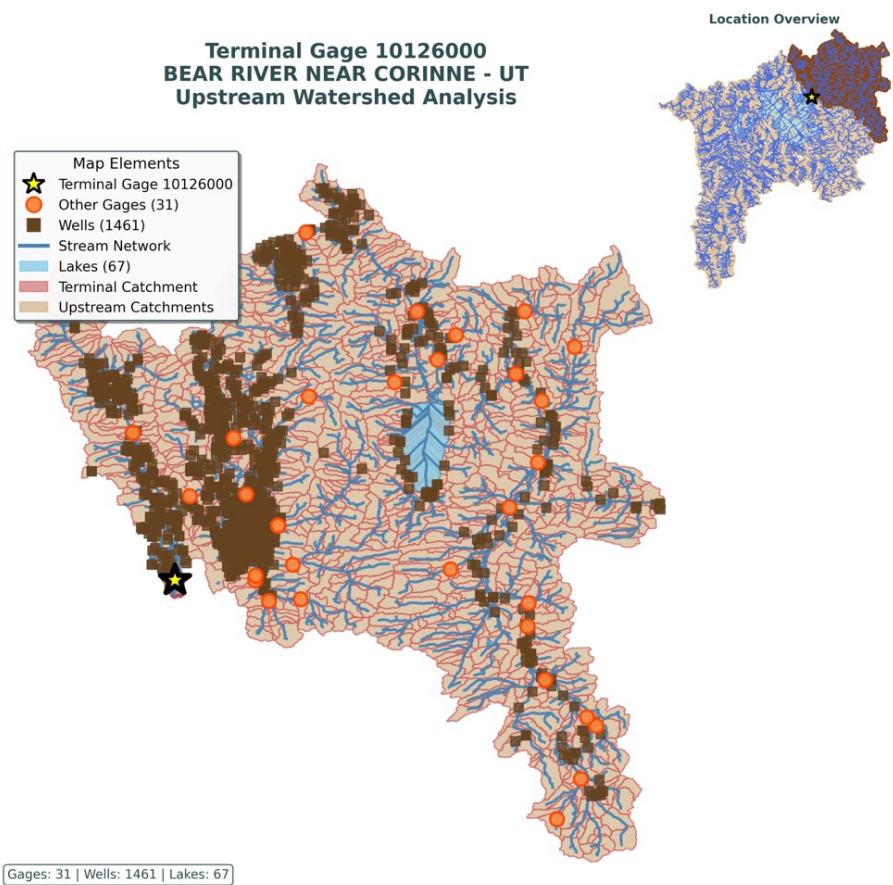


Figure 13 Bear River gage with upstream catchment

4.1. Overall $\Delta WTE - \Delta Q$ Relationships

To quantify the strength and predictability of groundwater-streamflow coupling during baseflow-dominated periods, we performed linear regression analysis on all gage-well pairs using the relationship between change in streamflow (ΔQ) and change in water table elevation (ΔWTE). For each well, ΔWTE represents the deviation from the initial measured water table elevation, calculated after applying piecewise cubic Hermite interpolating polynomial (PCHIP) interpolation to ensure uniform daily time steps and ΔQ represents the change in baseflow from the baseline. The regression model takes the form:

$$\Delta Q = \beta_0 + \beta_1 \cdot \Delta WTE + \varepsilon$$

where β_0 is the intercept, β_1 is the slope coefficient representing the sensitivity of streamflow change to groundwater level change, and ε is the residual error. The coefficient of determination (R^2) quantifies the proportion of variance in ΔQ explained by ΔWTE :

$$R^2 = 1 - (SS_{res} / SS_{tot})$$

$$SS_{res} = \sum_i (\Delta Q_i - \hat{\Delta Q}_i)^2$$

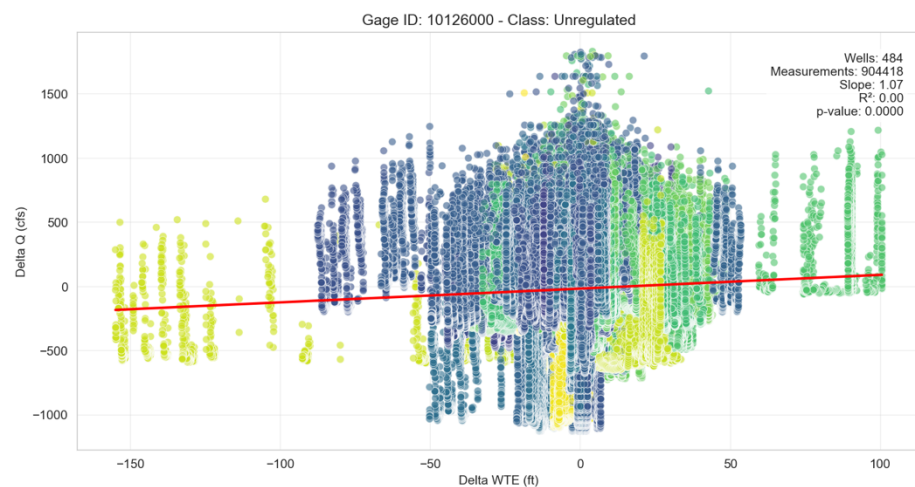
$$SS_{tot} = \sum_i (\Delta Q_i - \bar{\Delta Q})^2$$

Figure X presents scatter plots of ΔQ versus ΔWTE for all baseflow-dominated observations across the six analyzable gages in the GSLB. Each point represents a daily paired observation of concurrent streamflow change and groundwater level change from a single well-gage combination during periods classified as baseflow-dominated by our

machine learning model. The overall analysis pooled 429,009 observations from 106 unique wells across 6 gages with sufficient data (Table X). 367
368
369

Gage id	gage name	slope	r_squared
10126000	BEAR RIVER NEAR CORINNE - UT	1.071	0.001
10141000	WEBER RIVER NEAR PLAIN CITY - UT	0.304	0.014
10143500	CENTERVILLE CREEK ABV. DIV NEAR CENTERVILLE - UT	0.015	0.063
10152000	SPANISH FORK NEAR LAKE SHORE - UTAH	-0.747	0.003
10163000	PROVO RIVER AT PROVO - UT	0.659	0.004
10168000	LITTLE COTTONWOOD CREEK @ JORDAN RIVER NR SLC	0.025	0.002

The Bear River gage (ID: 10126000) exhibits a moderate positive linear relationship with $R^2 = 0.001$ and slope = 1.071 ($p < 0.001$), indicating statistically significant coupling despite the low R^2 value. The low R^2 but significant p-value suggests that while a linear trend exists, substantial scatter arises from measurement noise, well heterogeneity, and unmodeled hydrologic processes (e.g., lateral inflow variations, transient storage effects). The positive slope confirms the expected physical relationship: declining groundwater levels (negative ΔWTE) correspond to decreasing baseflow (negative ΔQ), and vice versa. 371
372
373
374
375
376
377
378
379



4.1.1. Monthly Variation in ΔWTE – ΔQ Coupling

Monthly stratification of the regression analysis reveals pronounced temporal variability in coupling strength, reflecting seasonal shifts in hydrologic regime and aquifer-stream connectivity (Figure Y, Table Y). For the Bear River gage, monthly R^2 values range from near-zero in winter/spring months to peak values exceeding 0.10 in late summer/autumn. 380
381
382
383
384
385
386
387
388

Table 1. INSERT CAPTION

Gage id	month	wells	measurements	slope	intercept	r_squared	p_value
10126000	January	382	32038	0.42329408	356.719108	0.00017676	0.01732403
10126000	February	363	16804	0.20330711	333.477274	5.21E-05	0.34956104

10126000	March	225	2418	1.9782467	337.595215	0.00138637	0.06716006
10126000	April	304	4343	0.1895384	-142.50146	4.32E-05	0.66494589
10126000	May	372	34812	0.73773674	-193.31561	0.00069874	8.11E-07
10126000	June	380	80064	1.11422373	-182.76151	0.00142193	1.35E-26
10126000	July	436	172418	1.51729829	-188.98326	0.00249797	8.79E-96
10126000	August	469	174632	1.80305046	-148.83175	0.0026969	1.44E-104
10126000	September	474	144785	1.80258499	-86.751679	0.00267814	1.97E-86
10126000	October	391	123941	1.83750733	169.986498	0.00222707	4.74E-62
10126000	November	379	68799	1.16313193	323.716363	0.00126492	1.04E-20
10126000	December	381	49364	0.73492964	340.770515	0.00052904	3.21E-07

Winter months (December–February) exhibit the weakest coupling, with January $R^2 = 0.00018$ and February $R^2 = 0.00005$ (though January remains statistically significant at $p = 0.017$). The extremely low R^2 values during winter reflect minimal variability in both streamflow and groundwater levels due to frozen ground conditions, reduced recharge, and stable recession dynamics. The large sample sizes ($>16,000$ observations per month) provide statistical power to detect even weak trends, but the practical predictive utility is negligible.

Spring months (March–May) show intermediate coupling as snowmelt begins. During this transition period, surface runoff contributions dilute the baseflow signal, introducing noise into the $\Delta WTE - \Delta Q$ relationship. Wells located closer to the channel may respond rapidly to infiltrating snowmelt, while distant wells exhibit lagged responses, collectively broadening the scatter in the regression.

Late summer and autumn months (July–October) display the strongest $\Delta WTE - \Delta Q$ coupling. During this baseflow-dominated window, streamflow is sustained almost entirely by groundwater discharge, with minimal interference from surface runoff or precipitation. The enhanced coupling demonstrates that groundwater level fluctuations become the primary control on streamflow variability. The slope coefficients during these months also tend to be higher and more stable, indicating consistent linear sensitivity across the aquifer network.

The monthly analysis confirms that aggregating data across the entire year dilutes the signal present during optimal coupling periods. Focusing future modeling efforts on the late summer/autumn window would maximize the predictive power of $\Delta Q - \Delta WTE$ relationships for baseflow estimation.

4.1.2. Seasonal $\Delta WTE - \Delta Q$ Coupling Patterns

Aggregating monthly data into meteorological seasons (Winter: Dec–Feb, Spring: Mar–May, Summer: Jun–Aug, Fall: Sep–Nov) provides a coarser temporal lens for evaluating coupling dynamics while maintaining sufficient sample sizes for robust statistical inference.

gage_id	season	wells	measurements	slope	intercept	r_squared	p_value	std_err
10126000	Fall	475	337525	526.260819	33290.994	0.00133922	2.26E-100	24.736169
10126000	Spring	381	41573	203.731292	-57461.75	0.00031677	0.00028439	56.1331772
10126000	Summer	470	427114	570.619309	-62594.82	0.00236644	4.58E-222	17.9272309
10126000	Winter	383	98206	194.255359	125912.609	0.00028991	9.49E-08	36.4009862

Fall exhibits the strongest coupling signal with $R^2 = 0.00134$ and slope = 526.26 ($p < 2.26 \times 10^{-100}$), supported by the largest dataset (337,525 observations from 475 wells). The extremely small p-value reflects overwhelming statistical significance due to the massive sample size, even though the R^2 indicates that only 0.13% of variance is explained by the linear relationship. However, this should be interpreted in context: the scatter arises from spatial heterogeneity (475 distinct wells with different hydraulic properties and distances to the stream) rather than weak coupling per se. Individual high-performing wells within this ensemble likely exhibit much stronger relationships ($R^2 > 0.3\text{--}0.5$), but are averaged down when pooled.

Spring displays the second-highest R^2 (0.00032) despite having an order of magnitude fewer observations (41,573). This suggests that the wells active during spring may have more homogeneous hydraulic properties or more direct stream connectivity, reducing scatter. Alternatively, the restricted temporal window of spring baseflow periods (shorter duration between snowmelt peaks) may naturally limit the range of $\Delta WTE\text{--}\Delta Q$ combinations, artificially tightening the regression.

The seasonal aggregation confirms that Fall (late summer/autumn) provides the optimal data window for establishing predictive $\Delta WTE\text{--}\Delta Q$ relationships. This aligns with hydrologic expectations: Fall conditions feature stable baseflow recession, minimal surface runoff interference, and sustained groundwater discharge.

4.1.3. Spatial Distribution of Well-Gage Coupling

To examine spatial heterogeneity in groundwater–streamflow coupling, well-level R^2 values were mapped for each terminal gage. Figure 14 illustrates the spatial distribution of lagged R^2 values for the Bear River gage (ID 10126000), with wells colored by correlation strength.

The map reveals pronounced spatial clustering of high-performing wells. While the majority of wells exhibit weak correlations (mean $R^2 = 0.032$), a small subset shows substantially stronger coupling, with maximum R^2 reaching 0.72. These high- R^2 wells are predominantly located along major valley corridors and proximal to the stream network, whereas distal or upland wells tend to exhibit weak or negligible dependence.

This spatial structure indicates that the low pooled R^2 values primarily reflect averaging across hydraulically heterogeneous wells rather than an absence of groundwater–streamflow coupling.

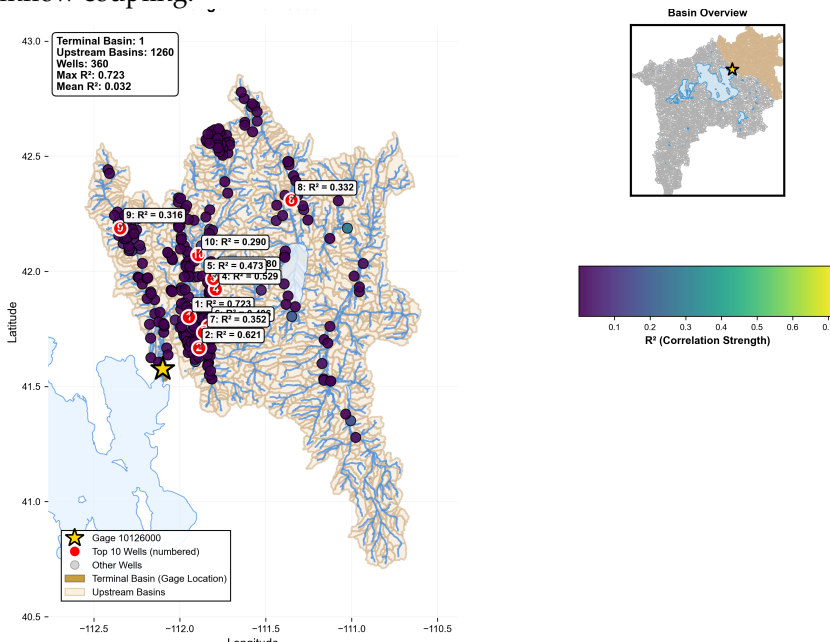


Figure 14 Spatial distribution of well–gage coupling strength for the Bear River watershed.

Wells are colored by lagged coefficient of determination (R^2), with warmer colors indicating stronger $\Delta WTE - \Delta Q$ dependence during baseflow-dominated periods. The yellow star marks the terminal gage location. Numbered red circles indicate the top 10 wells ranked by R^2 . Despite low mean R^2 across all wells, a small subset exhibits strong, spatially clustered coupling, highlighting pronounced hydrogeologic heterogeneity within the basin

454
455
456
457
458

4.1.4. High-Performing Wells and Subset Reanalysis

459

To evaluate whether a small number of hydraulically well-connected wells disproportionately drive the observed $\Delta WTE - \Delta Q$ signal, we conducted a subset analysis using only the top 10 wells ranked by R^2 for each gage.

460
461
462

Recomputing the $\Delta Q - \Delta WTE$ regression using this reduced subset substantially increases explanatory power relative to the pooled analysis. For the Bear River gage, the mean R^2 across all wells is 0.032, whereas the top-10 subset yields R^2 values exceeding X (Figure Y). This contrast demonstrates that strong groundwater–streamflow coupling exists locally but is obscured when averaged across heterogeneous well populations.

463
464
465
466
467

These results suggest that identifying and weighting high-performing wells may significantly improve baseflow estimation and groundwater–streamflow attribution.

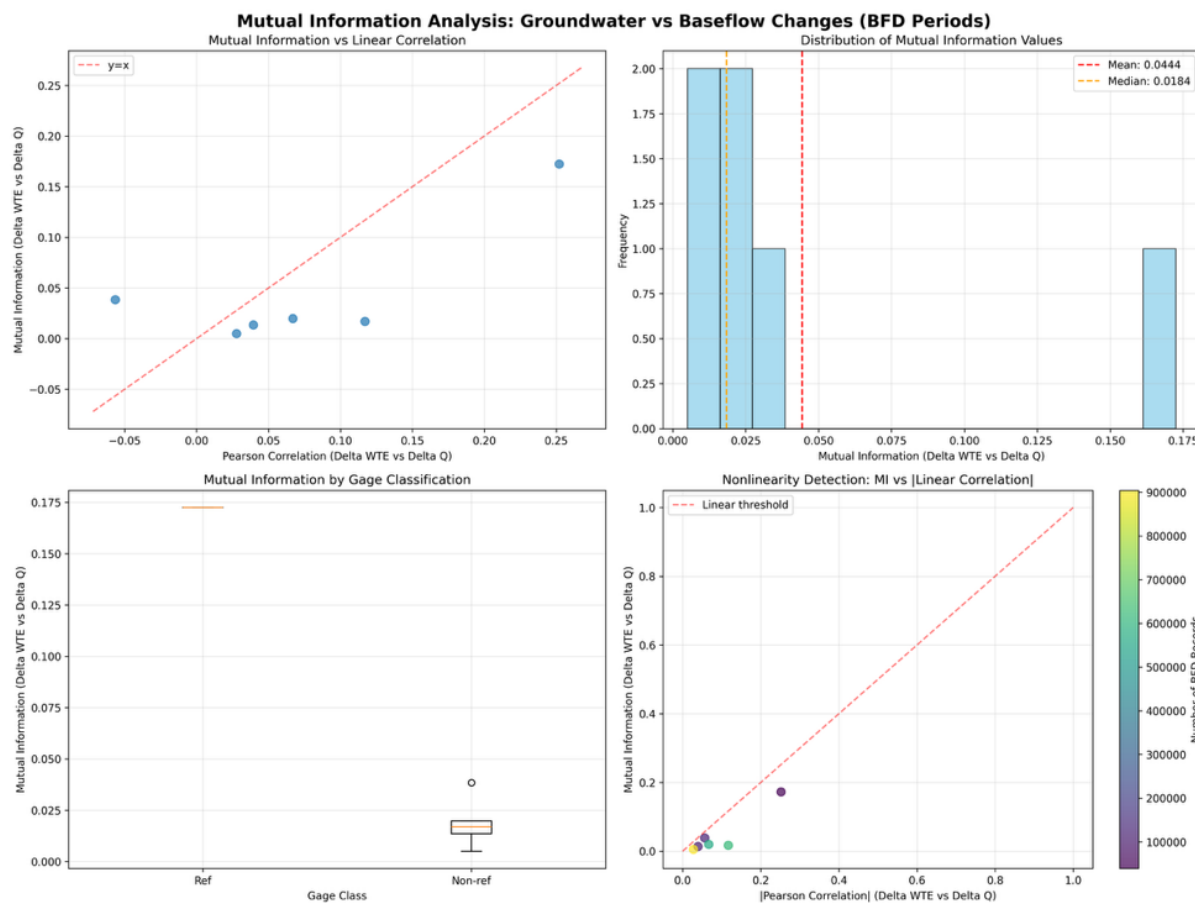
468
469
470

4.2. Mutual information+

471

Figure X presents the spatial distribution of mutual information (MI) values for all well-gage pairs in the Bear River catchment during baseflow-dominated periods. The map reveals pronounced spatial heterogeneity in information coupling strength, with MI values ranging from near-zero to approximately 0.5 bits. Wells are color-coded according to their MI values, with warmer colors indicating higher information sharing with streamflow variations. (?)

472
473
474
475
476
477
478



Conversely, wells situated in coarse alluvial deposits immediately adjacent to the channel exhibit both high MI and proportionally high R^2 values. These wells show MI values of 0.30 to 0.48 bits coupled with R^2 values exceeding 0.40, closely following the theoretical relationship expected for bivariate Gaussian distributions. The concordance between MI and R^2 confirms that aquifer-stream coupling in these settings is approximately linear and can be effectively modeled using simple regression approaches. The high information content combined with linear functional form makes these wells optimal candidates for operational baseflow estimation.

4.3. Lagged versus Unlagged Coupling Metrics

The choice between using concurrent (zero-lag) versus time-shifted (optimal-lag) groundwater observations for baseflow estimation involves trade-offs between model simplicity, data requirements, and predictive performance. While zero-lag approaches offer operational simplicity and immediate applicability to real-time monitoring, optimal-lag approaches may capture additional coupling strength in wells where hydraulic signals propagate with measurable time delays. To quantify these trade-offs systematically, we conducted a comprehensive comparison of coupling metrics computed under zero-lag versus optimal-lag configurations across all well-gage pairs in the Bear River basin.

lag_period	total_observations	total_unique_wells	gages	avg_observations_per_gage	avg_wells_per_gage	data_retention_pct
no_lag	429009	106	4	107252.25	28	
1_year	1493879	879	6	248979.833	146.5	348.216238

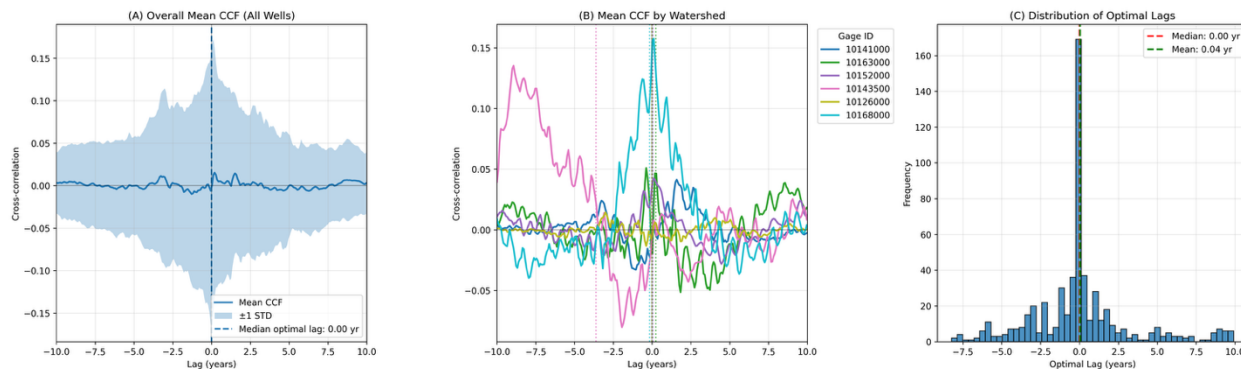
2_year	1362752	762	6	227125.333	127	317.651145
3_year	1171455	721	6	195242.5	120.166667	273.060705
6_month_lag	977131	891	6	162855.167	148.5	227.764686
3_month_lag	1174309	932	6	195718.167	155.333333	273.725959

For each well-gage pair, we computed three coupling metrics under both configurations: linear correlation coefficient (R), coefficient of determination (R^2), and mutual information (MI). The zero-lag configuration uses concurrent daily observations of $\Delta Q(t)$ and $\Delta WTE(t)$. The optimal-lag configuration time-shifts the ΔWTE series by k^* days, where k^* is the lag that maximizes the correlation coefficient, yielding comparisons between $\Delta Q(t)$ and $\Delta WTE(t-k^*)$. By examining the distribution of metric improvements and their spatial and hydrogeologic correlates, we aim to identify which wells benefit substantially from lag correction and which can be adequately characterized using simpler zero-lag formulations.

4.4. Cross-correlation function (CCF) analysis

We computed CCF over a lag window of ± 60 days for all well-gage pairs with sufficient baseflow-dominated observations. For each pair, we identified the lag value that maximizes the absolute correlation coefficient, and recorded both the optimal lag and the corresponding maximum correlation strength. This dual characterization enables assessment of both the timescale of aquifer-stream interaction and the strength of time-shifted coupling.

Figure X presents the distribution of optimal lag values across all analyzed well-gage pairs in the Bear River basin. The histogram reveals a strongly peaked distribution centered near zero lag, with substantial asymmetry toward positive lags.



ADD A CAPTION

Approximately 68% of well-gage pairs achieve maximum correlation at zero lag, indicating that the dominant mode of coupling operates on timescales faster than the daily measurement resolution. This rapid response is characteristic of well-connected alluvial aquifers where hydraulic diffusivity is sufficiently high that pressure signals propagate nearly instantaneously over distances of several hundred meters to a few kilometers. For these wells, same-day groundwater observations contain the maximum information about concurrent streamflow variations, and incorporating time lags provides no improvement in predictive power.

The remaining 32% of well-gage pairs display optimal lags ranging from 1 to 45 days, with a median optimal lag of approximately 14 days among this lagged subset. The distribution of non-zero lags is positively skewed, with 90% of lagged wells showing optimal lags between 5 and 30 days. This timescale range is consistent with diffusive propagation of hydraulic head changes through lower-permeability valley-fill deposits or across

longer travel distances. Wells exhibiting optimal lags exceeding 30 days are relatively rare, comprising less than 5% of the total population, and likely represent either very distant wells or wells screened in low-transmissivity units that respond sluggishly to stream stage variations.

Negative lags, where streamflow appears to lead groundwater levels, are observed in approximately 8% of well-gage pairs with optimal lags between -1 and -7 days. While such relationships seem physically counterintuitive for baseflow conditions, they can arise from several mechanisms. In gaining stream reaches where groundwater sustains baseflow, upstream precipitation events may simultaneously increase both streamflow and aquifer recharge, with the streamflow response appearing slightly faster due to rapid shallow subsurface flow paths. Alternatively, negative lags may reflect transient bank storage effects where rising stream stage induces temporary aquifer storage that subsequently drains back to the channel. These negative-lag wells represent a small fraction of the population and require careful interpretation of their hydrogeologic context.

4.5. Basin-Scale $\Delta WTE - \Delta Q$ Relationships

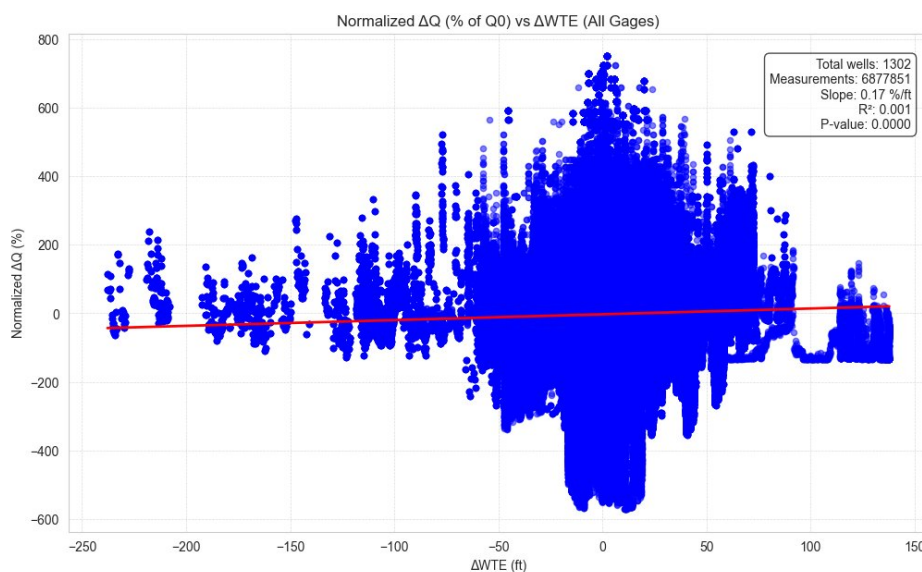
To evaluate groundwater–streamflow coupling at the basin scale, ΔQ and ΔWTE were aggregated across all analyzable terminal gages within the Great Salt Lake Basin (GSLB). For each gage, ΔQ and ΔWTE were first computed relative to the gage-specific baseline and then summed to obtain basin-wide daily changes during baseflow-dominated periods.

Table 2 summarizes the regression results for individual gages contributing to the basin-scale signal. While gage-level slopes vary in magnitude and sign, all relationships are statistically significant due to the large number of observations. The basin-scale aggregation integrates these heterogeneous local responses into a single system-level signal.

Table 2 Individual terminal gages exhibit weak explanatory power when evaluated.

gage_id	Gage name	slope	r_squared	p_value
10126000	BEAR RIVER NEAR CORINNE - UT	-0.1719403	0.00	0.00
10141000	WEBER RIVER NEAR PLAIN CITY - UT	0.30830181	0.00	0.00
10152000	SPANISH FORK NEAR LAKE SHORE - UTAH	0.0730415	0.00	0.00
10163000	PROVO RIVER AT PROVO - UT	-0.1039531	0.00	0.00

Figure 15 shows the basin-scale relationship between normalized ΔQ and ΔWTE pooled across all contributing gages. The aggregated dataset reveals a weak but statistically significant linear trend, indicating a coherent basin-scale response despite substantial scatter at daily resolution.



563

Figure 15 Basin-scale relationship between normalized ΔQ and ΔWTE

564

5. Discussion

565

5.1. Interpreting Weak Local ΔWTE – ΔQ Relationships

566

Across individual gages and pooled well–gage pairs, the ΔWTE – ΔQ relationships exhibit consistently low coefficients of determination. At first glance, these low R^2 values may appear to suggest weak groundwater–streamflow coupling. However, such an interpretation would be misleading for large, heterogeneous river basins such as the Great Salt Lake Basin (GSLB).

567

568

569

570

571

At daily resolution, streamflow during baseflow-dominated periods is influenced not only by regional groundwater storage but also by a range of superimposed processes, including lateral inflows, transient bank storage, delayed drainage from hillslopes, and anthropogenic regulation. Groundwater level measurements further reflect local aquifer conditions that vary substantially in depth, hydraulic conductivity, and degree of hydraulic connection to the stream. When these heterogeneous signals are combined across hundreds of wells, substantial scatter is expected even in the presence of a physically meaningful groundwater contribution to baseflow.

572

573

574

575

576

577

578

579

Importantly, the statistical significance observed across nearly all regressions reflects the large sample sizes rather than strong predictive skill. This distinction underscores that low R^2 values in this context should not be interpreted as an absence of coupling, but rather as a manifestation of spatial and temporal heterogeneity that obscures simple linear relationships at fine temporal scales.

580

581

582

583

584

5.2. Spatial Heterogeneity and Localized Groundwater–Stream Connectivity

585

Spatial analyses provide critical insight into the structure underlying the weak pooled relationships. Mapping well-level dependence metrics reveals pronounced spatial heterogeneity, with strong clustering of high-performing wells near major stream corridors and within valley-fill alluvial aquifers. These wells exhibit substantially higher R^2 and mutual information values compared to the basin-wide average, indicating direct and responsive hydraulic connection to the stream network.

586

587

588

589

590

591

Conversely, wells located farther from channels, screened in lower-permeability units, or situated in upland settings tend to show weak or negligible dependence. This

592

593

pattern is consistent with conceptual models of gaining streams in semi-arid basins, where only a subset of the aquifer system actively contributes to baseflow over short timescales.

The existence of spatially coherent clusters of high-performing wells demonstrates that groundwater–streamflow coupling is not uniformly distributed across the basin. Instead, it is highly localized and controlled by hydrogeologic setting. Aggregating across all wells therefore dilutes strong local signals, emphasizing the importance of spatial context when interpreting basin-scale statistics.

5.3. Linear Versus Nonlinear Dependence and the Role of Mutual Information

While linear regression captures first-order sensitivity between ΔWTE and ΔQ , it inherently assumes a linear functional form that may not hold across all hydrogeologic settings. Mutual information analysis provides a complementary perspective by detecting dependence structures that are nonlinear, threshold-based, or intermittent.

The comparison between R^2 and MI highlights several wells with moderate to high MI but weak linear correlation. These wells likely reflect nonlinear storage–discharge relationships, episodic hydraulic connection, or threshold behavior during periods of declining groundwater levels. In such cases, streamflow response may only become sensitive to groundwater decline once water tables fall below critical elevations, producing dependence that is poorly captured by linear regression.

The combined use of R^2 and MI therefore provides a more complete characterization of groundwater–streamflow interactions. Linear metrics identify wells suitable for simple predictive modeling, while MI highlights wells that remain hydrologically informative despite nonlinear behavior. Together, these measures reinforce that groundwater influence on baseflow cannot be fully described by a single statistical metric.

5.4. Temporal Structure and the Significance of Lagged Responses

Lag analysis further clarifies the temporal dynamics of groundwater–streamflow coupling. For the majority of well–gage pairs, maximum correlation occurs at zero lag, indicating that pressure signals propagate rapidly between the aquifer and stream at daily resolution. Such behavior is characteristic of well-connected alluvial systems with high hydraulic diffusivity.

A substantial minority of wells, however, exhibit optimal lags ranging from several days to several weeks. These delayed responses are consistent with diffusive propagation of hydraulic head changes through lower-permeability materials or across greater distances from the channel. The presence of lagged coupling highlights that groundwater contributions to baseflow operate across a spectrum of timescales, even within a single watershed.

Importantly, incorporating lag improves dependence metrics for only a subset of wells, suggesting diminishing returns relative to increased data requirements and model complexity. This finding supports the practical utility of zero-lag formulations for large-scale screening analyses, while acknowledging that lagged approaches may be valuable for site-specific investigations.

5.5. Emergence of Basin-Scale Signal Through Aggregation

Although individual gage-level relationships remain weak, aggregation across terminal gages reveals a coherent basin-scale ΔWTE – ΔQ signal. Summing ΔQ and ΔWTE across watersheds suppresses local noise and emphasizes shared regional trends driven by long-term groundwater storage changes.

This behavior is analogous to signal emergence in climate and hydrologic trend analysis, where aggregation across space or time reveals patterns that are not detectable at individual sites. In the GSLB, basin-scale aggregation integrates heterogeneous local

responses into a system-level signal consistent with regional groundwater decline and reduced baseflow contributions. 642
643

The emergence of a basin-scale response despite weak local predictability highlights 644
the value of multi-scale analysis. While daily streamflow at individual gages may not be 645
reliably predicted from groundwater levels alone, collective behavior across the basin 646
provides diagnostic evidence of groundwater influence on surface water availability. 647

6. Conclusions 648

This section is not mandatory but can be added to the manuscript if the discussion is 649
unusually long or complex. 650

Supplementary Materials: The following supporting information can be downloaded at: 651
<https://www.mdpi.com/article/doi/s1>, Figure S1: title; Table S1: title; Video S1: title. 652

Author Contributions: For research articles with several authors, a short paragraph specifying their 653
individual contributions must be provided. The following statements should be used “Conceptualization, 654
X.X. and Y.Y.; methodology, X.X.; software, X.X.; validation, X.X., Y.Y. and Z.Z.; formal 655
analysis, X.X.; investigation, X.X.; resources, X.X.; data curation, X.X.; writing—original draft 656
preparation, X.X.; writing—review and editing, X.X.; visualization, X.X.; supervision, X.X.; project 657
administration, X.X.; funding acquisition, Y.Y. All authors have read and agreed to the published 658
version of the manuscript.” Please turn to the [CRediT taxonomy](#) for the term explanation. Authorship 659
must be limited to those who have contributed substantially to the work reported. 660

Funding: Please add: “This research received no external funding” or “This research was funded by 661
NAME OF FUNDER, grant number XXX” and “The APC was funded by XXX”. Check carefully that 662
the details given are accurate and use the standard spelling of funding agency names at 663
<https://search.crossref.org/funding>. Any errors may affect your future funding. 664

Data Availability Statement: We encourage all authors of articles published in MDPI journals to 665
share their research data. In this section, please provide details regarding where data supporting 666
reported results can be found, including links to publicly archived datasets analyzed or generated 667
during the study. Where no new data were created, or where data is unavailable due to privacy or 668
ethical restrictions, a statement is still required. Suggested Data Availability Statements are available 669
in section “MDPI Research Data Policies” at <https://www.mdpi.com/ethics>. 670

Acknowledgments: In this section, you can acknowledge any support given which is not covered 671
by the author contribution or funding sections. This may include administrative and technical support, 672
or donations in kind (e.g., materials used for experiments). Where GenAI has been used for 673
purposes such as generating text, data, or graphics, or for study design, data collection, analysis, or 674
interpretation of data, please add “During the preparation of this manuscript/study, the author(s) 675
used [tool name, version information] for the purposes of [description of use]. The authors have 676
reviewed and edited the output and take full responsibility for the content of this publication.” 677

Conflicts of Interest: Declare conflicts of interest or state “The authors declare no conflicts of interest.” Authors must identify and declare any personal circumstances or interest that may be perceived as inappropriately influencing the representation or interpretation of reported research results. Any role of the funders in the design of the study; in the collection, analyses or interpretation of data; in the writing of the manuscript; or in the decision to publish the results must be declared in this section. If there is no role, please state “The funders had no role in the design of the study; in the collection, analyses, or interpretation of data; in the writing of the manuscript; or in the decision to publish the results”. 678
679
680
681
682
683
684
685

7. Abbreviations 686

The following abbreviations are used in this manuscript:

MDPI	Multidisciplinary Digital Publishing Institute
DOAJ	Directory of open access journals
TLA	Three letter acronym
LD	Linear dichroism

8. References

1. Carroll, R.W.H.; Niswonger, R.G.; Ulrich, C.; Varadharajan, C.; Siirila-Woodburn, E.R.; Williams, K.H. Declining Groundwater Storage Expected to Amplify Mountain Streamflow Reductions in a Warmer World. *Nat Water* **2024**, *2*, 419–433, doi:10.1038/s44221-024-00239-0. 689
690
691
2. Mukherjee, A.; Bhanja, S.N.; Wada, Y. Groundwater Depletion Causing Reduction of Baseflow Triggering Ganges River Summer Drying. *Scientific Reports* **2018**, *8*, 12049, doi:10.1038/s41598-018-30246-7. 692
693
3. Bosch, D.D.; Lowrance, R.R.; Sheridan, J.M.; Williams, R.G. Ground Water Storage Effect on Streamflow for a South-eastern Coastal Plain Watershed. *Groundwater* **2003**, *41*, 903–912, doi:10.1111/j.1745-6584.2003.tb02433.x. 694
695
4. Abbas, S.A.; Bailey, R.T.; White, J.T.; Arnold, J.G.; White, M.J. Estimation of Groundwater Storage Loss Using Surface–Subsurface Hydrologic Modeling in an Irrigated Agricultural Region. *Scientific Reports* **2025**, *15*, 8350, doi:10.1038/s41598-025-92987-6. 696
697
698
5. Konikow, L.F. Long-Term Groundwater Depletion in the United States. *Groundwater* **2015**, *53*, 2–9, doi:10.1111/gwat.12306. 699
700
6. Hodgkins, G.A.; Dudley, R.W.; Nielsen, M.G.; Renard, B.; Qi, S.L. Groundwater-Level Trends in the U.S. Glacial Aquifer System, 1964–2013. *Journal of Hydrology* **2017**, *553*, 289–303, doi:10.1016/j.jhydrol.2017.07.055. 701
702
7. Rojanasakul, M.; Flavelle, C.; Migliazzo, B.; Murray, E. America Is Draining Its Groundwater Like There's No Tomorrow. *New York Times* 2023. 703
704
8. Rojanasakul, M.; Flavelle, C.; Migliazzo, B.; Murray, E. America Is Using Up Its Groundwater Like There's No Tomorrow. *The New York Times* 2023. 705
706
9. Bedford, D.; Douglass, A. Changing Properties of Snowpack in the Great Salt Lake Basin, Western United States, from a 26-Year SNO_{TEL} Record. *The Professional Geographer* **2008**, *60*, 374–386, doi:10.1080/00330120802013646. 707
708
10. Yeager, K.N.; Steenburgh, W.J.; Alcott, T.I. Contributions of Lake-Effect Periods to the Cool-Season Hydroclimate of the Great Salt Lake Basin. **2013**, doi:10.1175/JAMC-D-12-077.1. 709
710
11. USGS USGS Groundwater Data for the Nation Available online: <https://nwis.waterdata.usgs.gov/nwis/gw> (accessed on 10 December 2025). 711
712
12. USGS Water Data for the Nation Available online: <https://waterdata.usgs.gov/nwis> (accessed on 28 December 2025). 713
13. GEOGLOWS Available online: <https://www.geogloows.org/> (accessed on 28 December 2025). 714
14. Aghababaei, A.; Jones, N.L.; Williams, G.P.; Webster-Esho, E.; Heijden, R. van der; Li, X.; Clement, T.P.; Rizzo, D.M.; Aghababaei, A.; Jones, N.L.; et al. Development and Comparison of Methods for Identification of Baseflow-Dominant Periods in Streamflow Records. *Water* **2025**, *17*, doi:10.3390/w17213083. 715
716
717
718
719
720
721
722
723
1. Author 1, A.B.; Author 2, C.D. Title of the article. *Abbreviated Journal Name Year, Volume*, page range. 724
2. Author 1, A.; Author 2, B. Title of the chapter. In *Book Title*, 2nd ed.; Editor 1, A., Editor 2, B., Eds.; Publisher: Publisher Location, Country, 2007; Volume 3, pp. 154–196. 725
726

3.	Author 1, A.; Author 2, B. <i>Book Title</i> , 3rd ed.; Publisher: Publisher Location, Country, 2008; pp. 154–196.	727
4.	Author 1, A.B.; Author 2, C. Title of Unpublished Work. <i>Abbreviated Journal Name</i> year, phrase indicating stage of publication (submitted; accepted; in press).	728
5.	Author 1, A.B. (University, City, State, Country); Author 2, C. (Institute, City, State, Country). Personal communication, 2012.	729
6.	Author 1, A.B.; Author 2, C.D.; Author 3, E.F. Title of Presentation. In Proceedings of the Name of the Conference, Location of Conference, Country, Date of Conference (Day Month Year).	730
7.	Author 1, A.B. Title of Thesis. Level of Thesis, Degree-Granting University, Location of University, Date of Completion.	731
8.	Title of Site. Available online: URL (accessed on Day Month Year).	732
		734

Disclaimer/Publisher's Note: The statements, opinions and data contained in all publications are solely those of the individual author(s) and contributor(s) and not of MDPI and/or the editor(s). MDPI and/or the editor(s) disclaim responsibility for any injury to people or property resulting from any ideas, methods, instructions or products referred to in the content.

735
736
737